X-ray intensity fluctuation spectroscopy studies of ordering kinetics in a Cu-Pd alloy

K. Ludwig,* F. Livet, F. Bley, and J.-P. Simon
LTPCM-ENSEEG-INPG, UMR-CNRS No. 5614, Boîte Postale 75-38402 Saint Martin d'Hères Cedex, France

R. Caudron
ONERA-LEM, Boîte Postale 72-29 Avenue de la Division Leclerc, 92322 Chatillon Cedex, France
and Laboratoire Léon Brillouin (CEA-CNRS), CEA Saclay, 91191 Gif-sur-Yvette, France

D. Le Bolloc'h
Laboratoire de Physique des Solides, UMR CNRS 8502, bât. 510, université Paris Sud, 91405 Orsay, France

A. Moussaid
ESRF, Boite Postale 220-38043, Grenoble, France
(Received 2 August 2005; published 10 October 2005)

X-ray intensity fluctuation spectroscopy has been used to examine the coarsening kinetics in the classic long-period superlattice Cu-Pd alloy. The evolution of the speckle intensity was examined near the centers of both a superlattice peak (associated with local $L1_2$ order) and a satellite peak (associated with one-dimensional antiphase correlations). The decay of the two-time correlation function $C(t_1,t_2,q)$ was independent of the direction examined and was similar for the superlattice and satellite peaks. In agreement with published Langevin theory and simulations, the decay time τ of the two-time correlation function increases linearly with average time $t_m=(t_1+t_2)/2$. It is relatively independent of the wave vector near the peak centers. However, τ increases much more slowly with increasing t_m than is expected.

DOI: 10.1103/PhysRevB.72.144201 PACS number(s): 61.66.Dk, 61.10.Eq, 64.60.Cn, 83.10.Tv

I. INTRODUCTION

X-ray intensity fluctuation spectroscopy (XIFS) continues to develop as an important tool for better understanding the evolution of condensed-matter systems on atomic and nanometer length scales.[1,2] Unlike traditional x-ray approaches, XIFS uses a small (typically $\sim 10\ \mu$m) x-ray beam that is sufficiently coherent to produce speckle patterns characteristic of the specific structural arrangement of the illuminated sample. XIFS examines the temporal evolution of the speckle pattern to reveal the underlying structural evolution of the material being studied. In this sense, it is quite analogous to dynamic light scattering (DLS). DLS requires optically transparent materials and typically probes length scales larger than the wavelength of visible light ($\sim$400 nm); it is unable to observe smaller defects. XIFS offers the possibility of observing ordering phenomena on length scales as small as 10 nm, with no restriction on optical transparency.

While a number of studies have used XIFS to examine fluctuation dynamics, fewer have attempted to use it to probe the kinetics of phase transitions.[3,4] This is also an area in which there have been few, if any, analogous DLS studies. Here we report a XIFS study of the ordering kinetics in the classic long-period superlattice alloy CuPd; the study measures the two-time pair-correlation function $C(q,t_1,t_2)$. This two-time correlation function contains information beyond that available from the ensemble-averaged one-time pair-correlation function (structure factor) $S(q,t)$ that is obtained from traditional time-resolved x-ray scattering experiments, such as we have recently performed on this alloy.[5] Our measurements probe the evolution of $C(q,t_1,t_2)$ in Cu-Pd on length scales of 10^1–10^3 nm and time scales of 10^2–10^4 sec. Such studies require high x-ray brightness—coming in these experiments from the undulator ID-10A Troïka beamline of the European Synchrotron Radiation Facility (ESRF)—and a relatively high scattering cross section—coming here from ordered domains of atoms. Our results are compared with existing theory and simulations[6] to better understand the coarsening process.

II. BACKGROUND—LONG-PERIOD SUPERLATTICE (LPS) ALLOYS

The Cu-rich Cu-Pd alloys exhibit structures based upon face-centered cubic (fcc) lattices. In the high-temperature disordered structure, Cu and Pd atoms occupy fcc sites at random, though short-range chemical order (SRO) can exist. In the simple $L1_2$ ordered structure with ideal stoichiometry Cu_3Pd, Cu atoms preferentially occupy face centers and Pd atoms preferentially occupy corners of the unit cell. Since there are four equivalent sites in the fcc unit cell, there is a factor of 4 degeneracy in the $L1_2$ ordered structure. Antiphase boundaries (APB's) between degenerate ordered regions can be either "conservative" or "nonconservative."[7] A conservative APB separates two ordered regions that differ from each other by a translation vector parallel to the plane of the APB interface. In this case, the local stoichiometry at the interface remains unchanged. A nonconservative APB separates two ordered regions that differ from each by a translation vector with a component perpendicular to the APB interface. In this case the local stoichiometry of the interface is changed. In the simple $L1_2$ structure region of a

phase diagram, there is a free-energy cost to forming APB's, and none exist in equilibrium. Because the nearest-neighbor atomic environment is not changed by the presence of conservative APB's, these are typically lower in energy than nonconservative APB's.

In contrast to the situation for the simple $L1_2$ structure, LPS alloy phases contain APB's as an integral part of their structure. Thus they exhibit a modulation of the order, with average domain size M between APB's. The Cu-Pd alloys are a classic LPS system with one-dimensional (1D) modulated structures at Pd concentrations of approximately 18–28 % and 2D modulated structures at elevated temperatures and Pd concentrations of approximately 24–32 %.[8] The APB's in the 1D LPS state are conservative, while in the 2D LPS state, one direction has conservative APB's and the other direction has nonconservative APB's. In both cases, the APB's are preferentially oriented along the cubic crystallographic axes. Below approximately 23% Pd, the 1D LPS states are incommensurate and have a period ($5 \leqslant M \leqslant 15$) which varies continuously with concentration and temperature. Above this composition the 1D LPS states are commensurate ($3 \leqslant M \leqslant 5$) and do not change much with temperature.

The diffraction pattern from a simple $L1_2$ structure exhibits "fundamental" Bragg peaks for which the crystallographic indices (hkl) are all of the same parity. These are independent of the degree of order, and thus exist even in the fcc disordered state. The $L1_2$ ordering also produces peaks at the "superlattice" reciprocal-lattice points where h, k, and l are not all of the same parity. If the ordering is imperfect, then the superlattice peaks will be broadened. However, because conservative APB's separate regions of order that differ by a vector that lies in the plane of the interface, their presence causes an anisotropic broadening of the superlattice peaks. Thus superlattice peaks in alloys with $L1_2$ order typically exhibit a "pancake" shape in reciprocal space, with the short dimension of the pancake—which we will refer to as the radial direction—being inversely proportional to the average distance between nonconservative APB's, and the long pancake dimension—which we will refer to as the transverse direction—inversely proportional to the average distance between a combination of conservative and nonconservative APB's.[7] In addition to the $L1_2$ superlattice peaks at appropriate integral reciprocal-lattice unit positions (i.e., as measured in units of $2\pi/a$), the reciprocal space structure of the 1D LPS phase of Cu-Pd alloys has satellite peaks separated from these by $q_0=(2M)^{-1}$ reciprocal-lattice units. The satellite peak widths are sensitive to the correlation length of modulated (long-period superlattice) order and depend on the specific phase relationships between the different sublattices on which ordering can take place. A simple model of the satellite peak widths is presented in Ref. 5.

III. EXPERIMENT

Experiments were carried out on the ID10A Troika beamline at ESRF. For this experiment, a Be lens was used to focus the beam and a Si (111) monochromator was used to select a 8.07-keV (1.54 Å) beam from the third harmonic of the undulator. The relative energy width was 1.4×10^{-4} full width at half maximum (FWHM). In a Gaussian wave packet $\exp[-r^2/\xi^2]$, this gives a longitudinal coherence length length $\xi_l=2(\ln 2)^{1/2}\lambda^2/\pi\Delta\lambda_{FWHM}\approx\lambda^2/2\Delta\lambda_{FWHM}\approx 1$ μm. Higher harmonics of the monochromator were suppressed by means of a small mirror. A 12-μm-diameter pinhole was used to define a coherent beam. The pinhole-sample distance was 0.23 m and the sample was 45 m from the source. Parasitic scattering from the pinhole was limited by guard slits, set to 20×20 μm, positioned halfway between the pinhole and the sample. A 1340×1300 pixel direct-illumination deep-depletion charge-coupled device (CCD) (Princeton Instruments) with a pixel dimension of $d=20$ μm was used as an area detector. The sample to detector distance was $R=2.25$ m. Thus each pixel corresponded to a reciprocal space width of approximately 3.6×10^{-4} nm^{-1}. The CCD detector was used in a photon counting mode.[9] By this method, we identify individual photons in each frame, and the resulting measured intensities are the number of x-ray photons absorbed in each pixel. The incident beam intensity was monitored using a small scintillation detector measuring the scattering of a thin kapton foil located after the beam defining pinhole. For each peak, 700 frames of data were collected, with an exposure time of 50 sec and a readout time of approximately 1.6 sec. Thus the evolution of the ordering was examined for an elapsed time of approximately 36 120 sec.

From the source size for the Troika beamline [900 μm horizontal by 23 μm vertical (FWHM)] and the above-mentioned energy spread, the transverse coherence area of the incident x-ray beam is estimated to be 6×220 μm ($H\times V$ FWHM) at the sample. At 2.3 m from the sample (i.e., the detector position) the speckle size corresponds to 36 μm (FWHM) which is slightly larger than the CCD pixel size. An approximate calculation gives an estimated incident beam coherence factor $\beta\approx0.3$ for the resulting x-ray beam. With the high monochromaticity of the beam, a small-angle experiment (SAXS) provides some check of this transverse coherence.[10,11] This has been done with an aerosyl sample in SAXS configuration. The incoherent scattering of the aerosyl is isotropic, and a careful study of the angular variations of the intensity provides an estimate of $\beta\approx0.20$ from the mean-square deviation relative to an angular average.

For large-angle experiments, coherence is reduced because of the limited longitudinal (temporal) coherence length. The difference in path length for scattering at a surface point on the sample and scattering at a point below the sample surface is $\delta r=l\sin^2\theta$, where l is the total path length in the sample. If we set $l\sim2\mu^{-1}\approx20$ μm, where μ^{-1} is the x-ray-absorption length in the material, then this gives a path difference $\delta r\sim0.8$ μm, which is comparable to the longitudinal coherence length. Detailed calculations assuming Gaussian or boxcar wave functions suggest that the difference in path lengths would be expected to lead to an effective decrease in coherence by a factor of approximately 30–40 %.

Experiments were performed on a (001) cut $Cu_{0.77}Pd_{0.23}$ single crystal grown at the Office National d'Etudes et de Recherches Aérospatiales (ONERA). The composition was verified by microprobe. During the real-time x-ray experiments, the sample was heated with a double-stage furnace

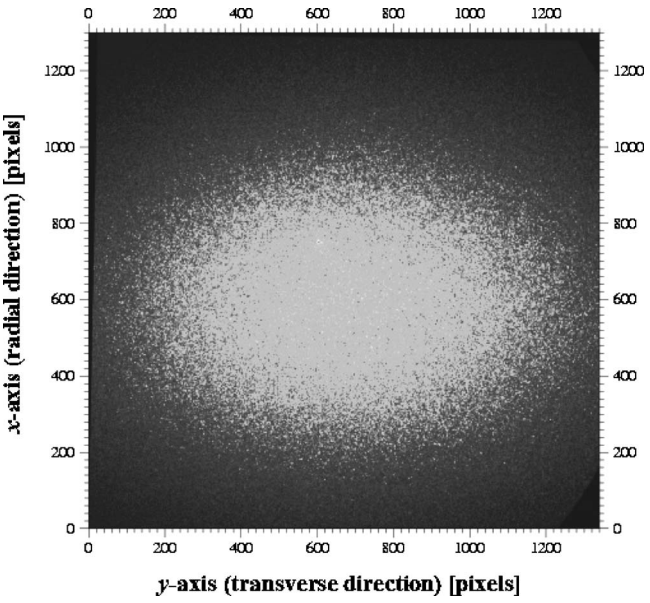

FIG. 1. Detector image of superlattice peak after 35 991 s of ordering. Dark regions around the image edge are due to masking of the scattered x rays.

inside a small high vacuum chamber with kapton windows to allow optimal x-ray access.

Samples were initially disordered at 510 °C, above the transition, and then rapidly (10 sec) quenched to a temperature of 435 °C. Data from two separate quenches are reported here. One data set was taken in the vicinity of the (001) superlattice peak—at $|q|=16.9$ nm$^{-1}=1$ r.l.u. (reciprocal-lattice unit) and incident angle $\theta=11.9°$. The second data set was taken near a neighboring satellite peak ($0\ q_0\ 1$), with $q_0 \approx 0.088$ r.l.u. For the scattering near the (001) superlattice peak, the CCD measured the x-ray scattered intensity on a small part of the Ewald sphere, approximately planar, with the x axis approximately in the crystal radial $[00l]$ direction and the y axis approximately in the transverse $[0k0]$ direction through the Bragg peak. For the satellite peak, the scattering geometry gave a slightly more complicated reciprocal space geometry.

It should also be noted that the range of wave vectors accessible with this experimental setup, coupled with the relatively slow coarsening kinetics, limited the reciprocal space region examined to to the central area of the peaks (i.e., within about ±1.5 standard deviations of the center). Thus the dynamics of the measured intensities in the CCD is only one order of magnitude, and the tails of the order peaks were not probed.

IV. RESULTS

A. Averaged scattering

In the late-stage coarsening regime the average domain size d_{avg} is expected to follow the Cahn-Allen[12] law $d_{avg}^2 = a(t-t_0) = at'$, where t_0 is a constant of integration. Therefore a common approach to determining the onset of coarsening is to examine the time evolution of a characteristic

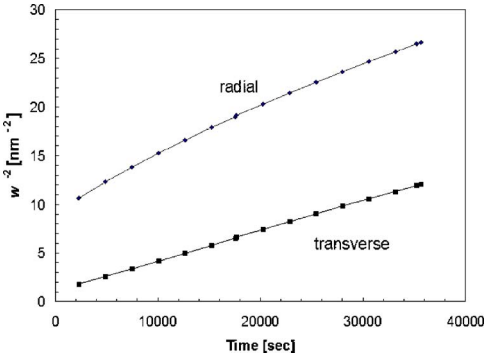

FIG. 2. (Color online) Evolution of superlattice inverse square width in radial and transverse directions.

wave vector q_c (often taken to be the FWHM of a superlattice peak) that is inversely proportional to the average domain size. For the case of the superlattice peak, a raw image of the superlattice peak is shown in Fig. 1. These were fit approximately by 2D Gaussian functions; the resulting inverse widths squared for the radial and transverse directions are displayed in Fig. 2. However, in determining the onset of coarsening behavior, ambiguities can arise, particularly in cases where the full three-dimensional reciprocal space intensity near the superlattice peak has not been measured. We therefore turned to a stronger requirement based upon dynamic scaling. It is expected that for an isotropic coarsening system with a nonconserved order parameter, the ensemble-averaged structure factor $S(q,t)$ should exhibit dynamic scaling[13] with

$$S(q,t) = q_c^{-3} F(q/q_c) = t'^{3/2} F(qt'^{1/2}), \tag{1}$$

where $t'=t-t_0$. As also discussed above, in the classic case of $L1_2$ alloys, the superlattice peaks are anisotropic. In this case the dynamic scaling must be modified to account for the different length scales in the two directions—radial and transverse. For the case of the (001) superlattice peak, l is the radial direction and h,k are the equivalent transverse directions. The radial l direction is nearly parallel to the x direction on the detector and the h direction is nearly parallel to the detector y direction. Since domain-wall dynamics affect the peak widths differently in the radial and transverse directions, in general t_{0x} will be different from $t_{0y}=t_{0z}=t_{0y,z}$ (here the x,y designations always refer to the direction on the detector as defined previously). Then the scaling form becomes

$$\begin{aligned} S(q_x,q_y,q_z,t) &= t_x^{1/2} t_y^{1/2} t_z^{1/2} F(q_x t_x^{1/2}, q_y t_y^{1/2}, q_z t_z^{1/2}) \\ &= t_x^{1/2} t_{y,z} F(q_x t_x^{1/2}, q_y t_{y,z}^{1/2}, q_z t_{y,z}^{1/2}), \end{aligned} \tag{2}$$

where $t_x=t-t_{0x}$ and $t_y=t_z\equiv t_{y,z}$ are similarly defined. It should be noted that, when the scattering follows this dynamic scaling form, the integrated scattering over the three-dimensional reciprocal space volume of the Bragg peak is guaranteed to be constant in time. For the satellite peak, our previous studies[5] have suggested that the peak symmetry is such that the peak widths in the plane of the four satellites surrounding a given superlattice point are comparable, but are quite different than the peak width perpendicular to that plane. In this case, Eq. (2) still holds approximately if "x" is

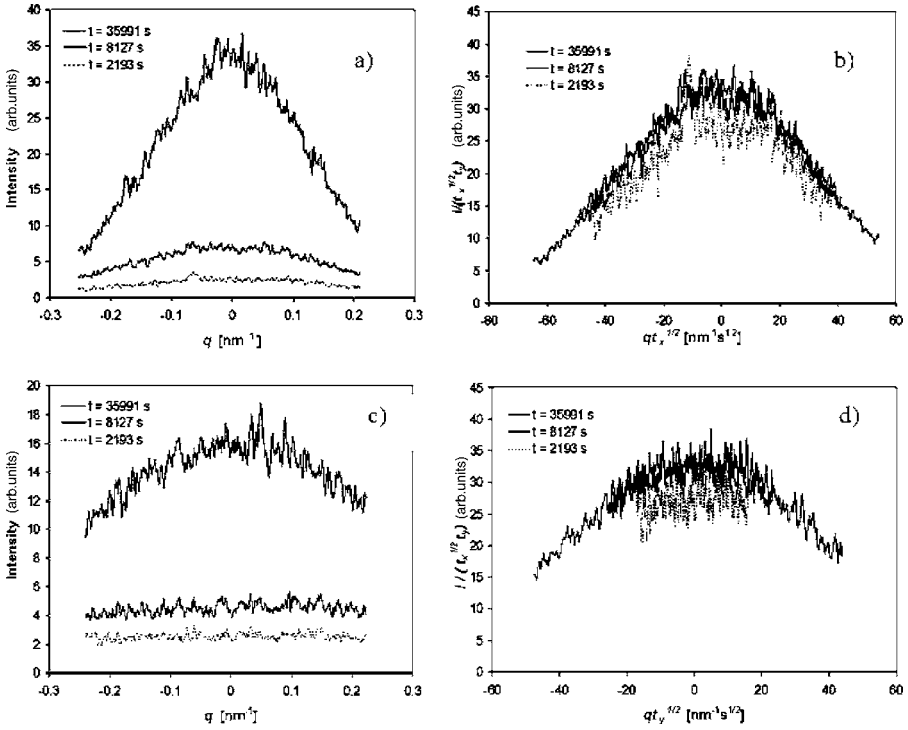

FIG. 3. (a) Superlattice intensities at three times along a center strip of pixels in the radial direction. The peak at approximately -0.06 nm^{-1} in the 2193-s data is due to a particularly large speckle. (b) Superlattice intensities scaled as described in the text. (c) Superlattice intensities at three times along a center strip of pixels in the transverse direction. (d) Scaled superlattice intensities. In both the radial and the transverse directions good scaling is observed after 5000–8000 sec.

taken to be the direction normal to the plane of the satellites.

In order to examine when the experimental $S(q,t)$ obeyed dynamic scaling for the superlattice and satellite peaks, the observed speckle intensities were separately averaged along strips ten pixels wide in the x and y directions. The unscaled intensities from the superlattice (001) peak in the radial direction are shown Fig. 3(a). For the superlattice peak, there are small relaxations in the radial and transverse peak positions (of order 2×10^{-2} nm^{-1}) during the ordering process. As discussed further below, a similar effect has also been reported recently in Cu_3Au, where it was suggested that it may be due to lattice distortions at the antiphase domain boundaries.[14,15] Lattice distortions at the domain boundaries would make the (001) peak asymmetric and shift the peak maximum in the *radial* direction. However, it is unclear how the *transverse* peak position could be affected by lattice distortions since there would remain a mirror symmetry about the axes in these directions. This is analogous to the well-known case of size-effect broadening in disordered alloys where the (001) peak can be shifted radially, but not transversely.[16] For the satellite peak, there is a much larger change of the transverse peak position $\delta q\approx8\times10^{-2}$ nm^{-1} during the ordering process, as we have observed in previous traditional time-resolved x-ray studies.[5] This is apparently due to a change in the average modulation wavelength during ordering.

To compare the radial data with the scaling form, the horizontal axes are scaled by $t^{1/2}$ and the vertical axes by $t_x^{-1/2}t_{y,z}^{-1}$. The scaled plots are shown in Fig. 3(b) using $t_{0x}=-30\,000$ s and $t_{0y,z}=-3000$ s; these offset values are in agreement with extrapolations of the data in Fig. 2 to the zero intercepts. The measured intensities exhibit good scaling after 5000–8000 s. Figures 3(c) and 3(d) show that there is simultaneous scaling in the transverse direction as well after 5000–8000 s. Similar results for the time of coarsening onset are obtained for the satellite peak. It is noteworthy that these offset times are sufficiently large to significantly restrict the range of the effective coarsening times $t_{x,y,z}$ examined.

We conclude, then, that the coarsening kinetics appears to be consistent with the Cahn-Allen prediction and with the dynamic scaling predicted for systems with a nonconserved order parameter, despite the complexities of the LPS structure. This is in agreement with our previous work.[5] It is noteworthy that theoretical investigations of coarsening in axial next-nearest-neighbor Ising (ANNNI) models have also found agreement with the Cahn-Allen $w\sim t^{1/2}$ prediction.[17,18]

B. XIFS

Having addressed the applicability of dynamic scaling to the ensemble averaged structure factor $S(q,t)$, we can now examine the behavior of the fluctuations about the ensemble average. Because the speckle patterns evolved relatively slowly over time, CCD frames were binned together by 10 to improve statistics.

To calculate the two-time correlation function, we begin by examining the normalized intensity fluctuation:

$$D(q,t)=\frac{I(q,t)-\langle I(q,t)\rangle}{\langle I(q,t)\rangle}. \tag{3}$$

Calculating $D(q,t)$ requires the determination of the ensemble average intensity $\langle I(q,t)\rangle$ for each pixel and time. This is the intensity measured in the incoherent experiment. This was estimated by smoothing the observed speckle pattern using an algorithm with a weighted averaging of each pixel with its nearest neighbors. This algorithm was iterated approximately 1000 times to produce relatively smooth structure factors. Due to the central limit theorem, this is

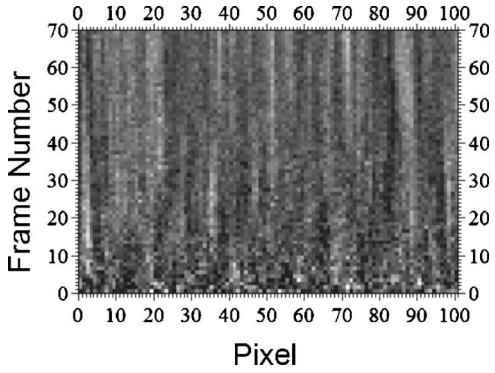

FIG. 4. Evolution of pixel intensities near the center of the superlattice peak. With increasing coarsening, the speckles become longer lived. Each binned frame corresponds to an elapsed time of 516 sec.

roughly equivalent to convoluting our intensity with a Gaussian of about 30 pixels FWHM. The normalized intensity fluctuations $D(q,t)$ were then calculated for each pixel.

The theoretical work of Brown *et al.*[6] predicts that, with increasing time, the speckles themselves become longer lived. Indeed comparison of speckle patterns over the period of the experiment shows that individual speckles develop with lifetimes comparable to the duration of the experiment. This increase in speckle lifetime can be seen in Fig. 4, where the pixel intensity is plotted as a function of time for a section of the detector near the superlattice peak center.

During the course of the experiment small motions of the incident beam due to small changes in the electron beam position in the storage ring can alter the observed scattering pattern independently of any structural changes occurring in the sample. To first approximation, small changes in incident beam angle shift the entire speckle pattern on the detector if the change in the angle is perpendicular to the scattering plane. If the change in angle is not perpendicular to the scattering plane, then it is still true that beam motion causes a shift if the speckles are significantly longer in the radial direction than in the transverse direction. This is indeed expected to be the case here as the penetration depth into the sample $(\mu^{-1}\sin\theta)/2\sim 1\ \mu$m is much smaller than the footprint on the sample $(12\ \mu\text{m}/\sin\theta\sim 58\ \mu\text{m})$. Such small shifts can be occasionally seen by the eye. As a particularly large example, Fig. 5 shows a shift of the speckle pattern by approximately one pixel between two subsequent frames. While we did not find it absolutely necessary to correct for these small shifts to obtain reasonable two-time correlation functions $C(q,t_1,t_2)$, the behavior of the functions was improved by implementing the corrections described here. Each $D(q,t)$, in the time sequence of detector frames was compared to the speckle pattern $D(q,t_{middle})$ measured at the middle of the time sequence. Before further analysis, each pattern was shifted slightly to maximize the overlap sum $\Sigma_q D(q,t)D(q,t_{middle})$. To estimate the shifted pattern for fractional translations, a 2D quadratic function was used for interpolation. The nine parameters for the quadratic were obtained by requiring that it pass through a central pixel and its eight nearest and next-nearest neighbors. In most cases, frame shifts smaller than one pixel were necessary. In some cases, shifts appeared to be gradual, while in other cases (most dramatically shown in Fig. 5), shifts occur on the time scale of individual frames. The shifts were not applied at the earliest times because the speckle patterns change sufficiently quickly that the overlap sum was not deemed reliable.

After obtaining the optimal shifts, the products $D(q,t_1)D(q,t_2)$ were calculated at each pixel. The average of the product of the normalized intensity fluctuations gives a two-time correlation function:

$$C(q,t_1,t_2) = C(q,\Delta t,t_m) = \langle D(q,t_1)D(q,t_2)\rangle_{equivalentq}, \quad (4)$$

where the average is over equivalent wave vectors, and we have introduced $\Delta t = t_2 - t_1$ and $t_m = (t_1+t_2)/2$. The evolution of the correlation function was examined independently along the x and y directions to study any kinetic anisotropy. To gain statistical accuracy, the bins of "equivalent wavevector" pixels were chosen to be 70 pixels in radial width (corresponding to 0.025 nm^{-1} in reciprocal space) and to incorporate only those pixels within 17° of the axis of interest. The use of other binning arrangements did not affect the analysis results. For simplicity, when referring to wave number below, we will quote the value at the center of the relevant bin. The "zero" wave vector is taken to be the peak center.

As was noted above, however, the peak centers move a small amount during the coarsening process. Examination of the speckle patterns shows that the speckles themselves do not follow this motion—rather they remain relatively fixed on the detector while speckle maxima in the direction of

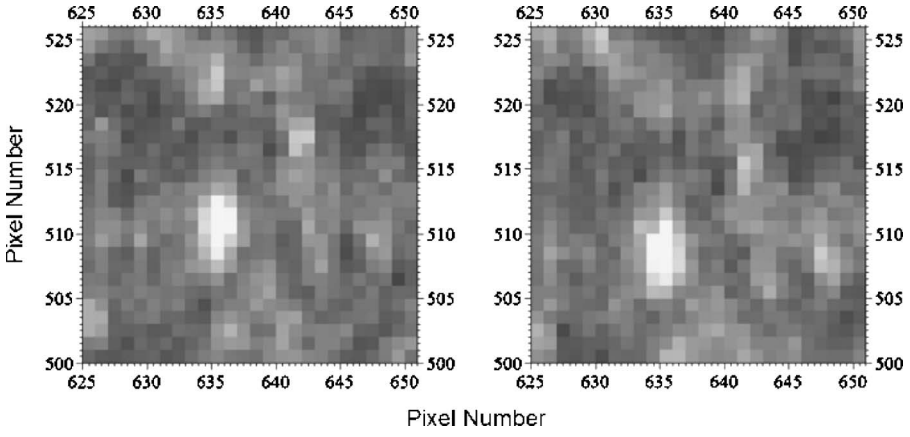

FIG. 5. Shift of satellite speckle pattern by approximately one pixel downward observed between frames at 33 280 s (left) and 33 800 s (right).

peak motion tend to grow more than do those in the opposite direction. This would be difficult to explain if the motion of the peaks were due to sample motion (tilting) during the ordering process. Instead we turn to a more microscopic viewpoint. The scattering that we are observing is dominated by correlations between antiphase domains. If the entire lattice were to expand or contract uniformly without altering the geometry of the domains, the speckle pattern would simply expand or contract relative to the origin of reciprocal space. This is not what is observed—the peak centers shift, but not the speckle patterns. This would appear to be consistent with the conjecture that the shifts are associated with lattice distortions inhomogeneously distributed in the sample at domain boundaries.[15] To analyze the speckle patterns, an average center was therefore chosen and held fixed.

For $\Delta t=0, C(q,t_1,t_2)$ is the sum of a term due to Poisson noise from the photon statistics and one due to the coherence factor β. The first term can be removed from the data by extrapolating from neighboring time bins $t\pm\delta t$. With increasing $\Delta t, C(q,\Delta t,t_m)$ decays to zero. For a system in equilibrium, $C(q,\Delta t,t_m)$ will be independent of t_m and its behavior can be related to the dynamics of equilibrium fluctuations. For a nonequilibrium system, however, the two-time correlation function will in general change with time as the system evolves.

During the data analysis process, there are several methods to evaluate the degree of coherence of the scattered x rays. As mentioned above, the coherence measured in a SAXS pattern from an aerogel gave a coherence factor in the scattered beam of $\beta\approx 0.20$. However, for the wide angle scattering experiment, we can expect significantly reduced β due to the penetration of the beam into the sample and the slightly asymmetric scattering geometry. One way to calculate β is from the variations of intensity among pixels for which the average structure factor should be approximately constant:

$$\beta = \frac{\langle I^2(q,t)\rangle - \langle I(q,t)\rangle}{\langle I(q,t)\rangle^2} - 1. \tag{5}$$

Another method is by examining the limit of the two-time correlation function:

$$\beta = \lim_{t_1\to t_2} C(q,t_1,t_2), \tag{6}$$

where the limit avoids the Poisson noise present for $t_1=t_2$. Both calculations are in agreement and give a value of 0.03–0.04 %. This is considerably reduced from the value of $\beta \approx 0.20$ observed with this incident beam in SAXS patterns from aerosyl. Since calculations of the effect of finite penetration into the sample suggest that the coherence of the scattered beam should be decreased by approximately 30–40 %, it is unclear why the measured value of β is reduced so much here.

In order to remove the effects of the imperfect coherence, it is convenient to follow earlier work[3,4,6] by normalizing the two-time correlation function:

$$C_{norm}(q,t_1,t_2) = \frac{2C(q,t_1,t_2)}{[C(q,t_1,t_1-\delta t)+C(q,t_1,t_1+\delta t)]^{1/2}[C(q,t_2,t_2-\delta t)+C(q,t_2,t_2+\delta t)]^{1/2}}, \tag{7}$$

where δt is the time step between recorded frames. By construction, the function is symmetric in t_1 and t_2. Contours of $C_{norm}(q,t_1,t_2)$ near the (001) superlattice peak are shown in Fig. 6. Figure 7 shows slices through the correlation functions at particular values of t_1 for different directions and wave numbers for both the superlattice and satellite peaks. As can be observed qualitatively in Figs. 6 and 7, and as predicted by theory, correlations become longer lived with increasing time following the quench. Moreover, in this wave-number regime, there appears to be little, if any, difference between the correlation functions in different directions, different wave numbers, or for different peaks (superlattice vs satellite).

We now quantitatively examine how correlation times grow. As mentioned above, Brown *et al.*[6] have used analytical Langevin theory and simulations to examine the behavior of $C(q,\Delta t,t_m)$ for the late-stage coarsening regime in phase ordering systems with nonconserved order parameters. Their work suggests that, in the coarsening regime, $C(q,\Delta t,t_m)$ should obey scaling laws. In particular, they predict that a scaling variable $x=q^2t$ exhibits two regimes of behavior. For

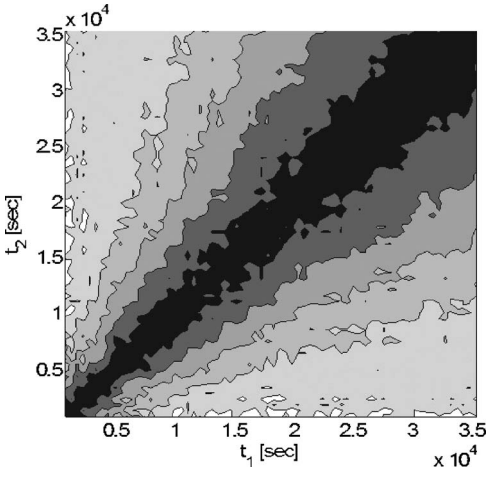

FIG. 6. Contour plot of the normalized two-time correlation function $C_{norm}(q=0.0126\ \mathrm{nm}^{-1},t_1,t_2)$ for the superlattice peak. Contours are at 0.2 intervals, with the highest contours being >0.8.

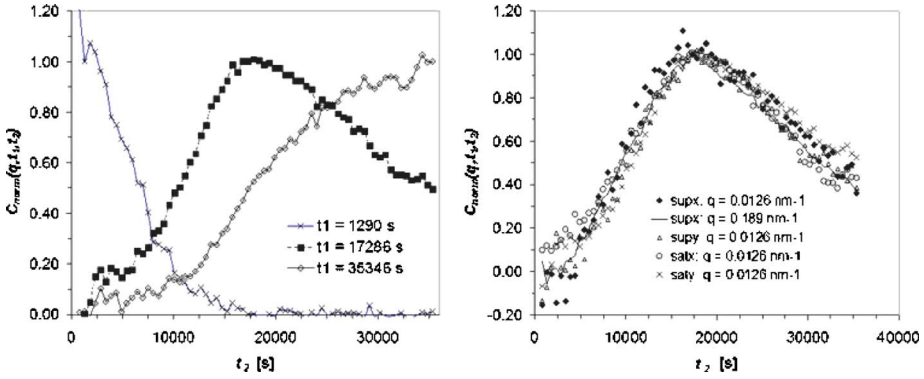

FIG. 7. (Color online) Normalized two-time correlation functions $C_{norm}(q,t_1,t_2)$ for the satellite and superlattice peaks. (a) $C_{norm}(q=0.0126\ \mathrm{nm}^{-1},t_1,t_2)$ for the satellite peak in the detector x direction shown at three times t_1 near the beginning, middle, and end of the experiment. (b) $C_{norm}(q,t_1,t_2)$ at approximately 17 286 s for the superlattice (sup) and satellite (sat) peaks in the detector x and y directions.

small $x_m=q^2t_m$, the characteristic decay time of the two-time correlation function, $x_\tau=q^2\tau$, is predicted to be linear in x_m. For large x_m, it is predicted that $x_\tau\sim x_m^{1/2}$. In this latter regime, it is predicted that the two-time correlation function decays as

$$C_{norm}(z)=[z^2K_2(z)/2]^2, \tag{8}$$

where $K_2(z)$ is a modified Bessel function of the second kind and a different scaling variable is introduced: $z=A\Delta t/t_m^{1/2}$, where A makes the variable dimensionless. Although this equation strictly only applies for large x_m, it appears to work well for all times measured in these experiments and provides an accurate way of estimating the FWHM correlation decay time τ. In determining τ, fits can be made to the data at constant t_1, or at constant t_m; similar results are obtained in either case. Representative fits at constant t_m are shown in Fig. 8. This figure again shows that the correlation decay time increases with increasing t_m.

Figure 9 shows the fit decay times for the superlattice and satellite peaks as a function of average time t_m for different wave vector and directions. The increase of correlation times is approximately linear with t_m, as predicted by theory. Moreover, for the relatively small wave vectors studied here (within ±1.5 standard deviations of the peak center), the decay times depend little, if at all, on the wave vector. As expected from the previous graphs, there appears to be little, if any, difference between the behavior of the superlattice and satellite peaks.

As discussed above, theory is usually expressed in terms of the scaling variable $x=q^2t$. Figure 10 shows the resulting scaled variables for the superlattice peak in the radial (x) direction. As predicted by theory for this wave-number range, the graph is linear with a slope of unity (as suggested by the linear behavior observed in Fig. 9). Quite similar results are obtained for the correlation decay time in the y direction and for correlation decay times in the two orthogonal directions for the satellite peak.

V. DISCUSSION AND CONCLUSIONS

The XIFS results presented here show that, during the coarsening process, both the $L1_2$ ordering (i.e., that associated with the superlattice peaks) and the 1D LPS ordering exhibit increasingly long structural correlations as measured by the two-time correlation function. The behavior of the two-time correlation function is very similar for the two types of order. This may reflect the fact that local $L1_2$ order is a prerequisite for forming the 1D LPS phase. The correlation time τ increases linearly with t_m as predicted by theory[6] for the low-wave-number regime.

One notable difference between previous theory and simulations and these experiments, however, is the signifi-

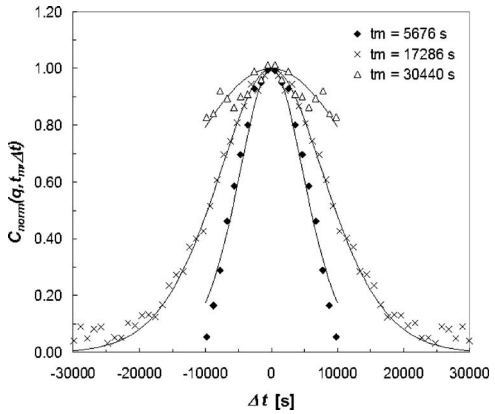

FIG. 8. Normalized two-time correlation functions $C_{norm}(q=0.0126\ \mathrm{nm}^{-1},t_m,\Delta t)$ for the satellite peak in the y direction for three different mean times t_m. Lines are fits to the theoretical line shape of Eq. (8).

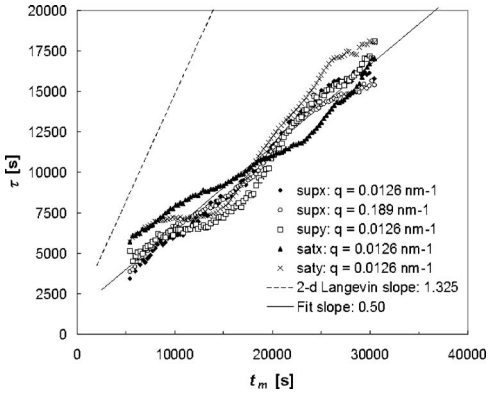

FIG. 9. Half width decay time τ of the normalized two-time correlation functions $C_{norm}(q,t_m,\Delta t)$ for the superlattice and satellite peaks as a function of the mean transformation time t_m. Also shown are lines with the 2D Langevin slope and data fit slope.

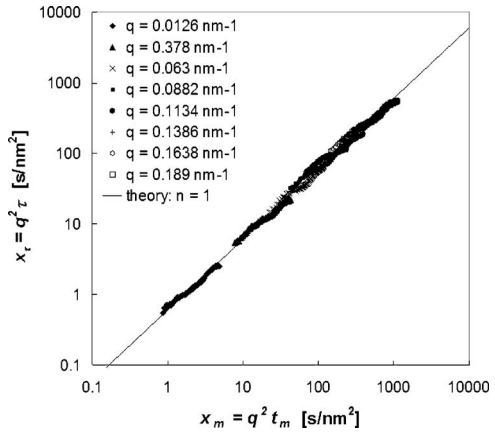

FIG. 10. Scaled correlation time $q^2\tau$ as a function of scaled mean coarsening time q^2t_m for the superlattice peak in the radial (x) direction. The power-law slope is in good agreement with the theoretical prediction of unity when near the peak center.

cantly slower growth of the correlation decay time τ with increasing t_m average time observed in the experiment. This ratio is a dimensionless quantity. Langevin calculations and simulations give a ratio of 1.325 in two dimensions. In three dimensions, the Langevin model would give a slightly higher ratio. In contrast, the observed ratios in both the superlattice and the satellite peaks are approximately 0.50 in both perpendicular directions. Interestingly, a recent XIFS study[14,15] of coarsening in Cu_3Au finds a ratio of approximately 0.75—significantly less than predicted by theory and simulation but somewhat greater than that observed here. It is unclear what properties of the system this ratio depends upon. The elapsed time is proportional to the square of average domain size and the correlation time measures the rate of structural rearrangements in the crystal. This ratio therefore might be viewed as measuring how efficiently structural rearrangements lead to average domain growth with increasing coarsening. The low measured ratio suggests that the growing average domain size leads to more structural rearrangement than is the case in the Langevin model. It is difficult to understand why this would be the case. However, in evaluating the veracity of the results, it should be noted that they have been reproduced in two separate quenches (one used to examine the superlattice peak and the other to examine the satellite peak), that the correlation times are indeed linear with t_m as predicted by theory and simulation, and that similar disagreement between experiment and theory has been observed by Fluerasu *et al.*[14,15]

In order to investigate the issue further, we have performed 2D simulations on model systems. Nearest-neighbor Ising-model simulations with spin-exchange dynamics were performed with quenches from random configurations to $0.8T_c$ and $0.9T_c$. In both cases, the two-time correlation decay times behave in excellent agreement with the Langevin model. We also examined an Ising model with vacancy-mediated dynamics. Again, the results appear to be generally consistent with Langevin predictions. Finally, in order to examine the effect of ground-state degeneracy, we examined a model with an A_3B concentration ratio, interactions to the third neighbor, and spin-exchange dynamics. The interactions were chosen to stabilize an ordered structure that has rows in each axis direction that alternate between pure A and $50\%A+50\%B$. In the mixed rows, the A and B atoms alternate. This structure is, in some ways, a 2D analog of the $L1_2$ ordered structure; it has a fourfold degeneracy, partially ordered structures can exhibit conservative and nonconservative domain walls, and the superlattice peaks are anisotropic. However, in this case we again found that the two-time correlation function decay times are in general agreement with Langevin predictions.

Another possibility for the difference between experiment and theory and simulations is that local lattice distortions at domain walls (possibly evidenced by the evolving peak center) may play a role in kinetics that is not captured in the theory and lattice simulations. However, these would presumably affect local structure—not the larger scale structure probed at the wave numbers examined in this experiment. It is unclear, moreover, how the observed small superlattice peak shift might be related to such distortions. As discussed above, the relatively fixed speckle positions suggest that the peak shifts are not associated with a homogeneous lattice relaxation, consistent with the hypothesis of an inhomogeneous lattice distortion relaxation at domain walls. However, it is unclear how such a mechanism could lead to the observed (001) peak motion in the transverse direction. Clearly, we still have something new to learn from XIFS studies of kinetics in alloys.

ACKNOWLEDGMENTS

We would like to thank Didier Regen and Denis Boivin for preparation and characterization of the samples. We thank Troika staff members Federico Zontone, Patrick Feder, and Henri Gleyzolle for their beamline help. We gratefully acknowledge discussions with Mark Sutton and Andrei Fluerasu and for their sharing of their work prior to its publication. We thank the European Synchrotron Radiation Facility for access to the Troika beamline ID10A. We would like to acknowledge partial support of this research by NSF Grant No. DMR-0508630.

*Permanent address: Deptartment of Physics, Boston University, Boston, MA 02215.

[1] M. Sutton, S. E. Nagler, S. G. Mochrie, T. Greytak, L. E. Bermann, G. Held, and G. B. Stephenson, Nature (London) **352**, 608 (1991).

[2] S. Brauer, G. B. Stephenson, M. Sutton, R. Bruning, E. Dufresne, S. G. J. Mochrie, G. Grubel, J. Als-Nielsen, and D. L. Abernathy, Phys. Rev. Lett. **74**, 2010 (1995).

[3] A. Malik, A. R. Sandy, L. B. Lurio, G. B. Stephenson, S. G. J. Mochrie, I. McNulty, and M. Sutton, Phys. Rev. Lett. **81**, 5832

(1998).
[4] F. Livet, F. Bley, R. Caudron, E. Geissler, D. Abernathy, C. Detlefs, G. Grubel, and M. Sutton, Phys. Rev. E **63**, 036108 (2001).
[5] X. Wang, J. Mainville, K. Ludwig, X. Flament, A. Finel, and R. Caudron, Phys. Rev. B **72**, 024215 (2005).
[6] G. Brown, P. A. Rikvold, M. Sutton, and M. Grant, Phys. Rev. E **56**, 6601 (1997).
[7] B. E. Warren, *X-ray Diffraction* (Dover, New York, 1990).
[8] P. R. Subramanian and D. E. Laughlin, J. Phase Equilib. **12**, 231 (1991).
[9] F. Livet, F. Bley, J. Mainville, M. Sutton, R. Caudron, S. G. J. Mochrie, E. Geissler, G. Dolino, D. L. Abernathy, and G. Grübel, Nucl. Instrum. Methods Phys. Res. A **451**, 596 (2000).
[10] D. L. Abernathy, G. Gruebel, S. Brauer, I. McNulty, G. B. Stevenson, S. G. J. Mochrie, A. R. Sandy, N. Mulders, and M. Sutton, J. Synchrotron Radiat. **5**, 37 (1998).
[11] F. Livet, F. Bley, A. L'eboublon, J. P. Simon, and J. F. B'erar, J. Synchrotron Radiat. **5**, 1337 (1998).
[12] S. M. Allen and J. W. Cahn, Acta Metall. **27**, 1085 (1979).
[13] T. Ohta, D. Jasnow, and K. Kawasaki, Phys. Rev. Lett. **49**, 1223 (1982).
[14] A. Fluerasu, M. Sutton, and E. M. Dufresne, Phys. Rev. Lett. **94**, 055501 (2005).
[15] A. Fluerasu, Ph.D. thesis, McGill University, 2003.
[16] B. Borie and C. J. Sparks, Acta Crystallogr., Sect. A: Cryst. Phys., Diffr., Theor. Gen. Crystallogr. **A27**, 198 (1971).
[17] T. Ala-Nissila, J. D. Gunton, and K. Kaski, Phys. Rev. B **33**, 7583 (1986).
[18] T. Ala-Nissila, J. D. Gunton, and K. Kaski, Phys. Rev. B **37**, 179 (1988).